Engineering Geology 128 (2012) 12–22

Contents lists available at SciVerse ScienceDirect

Engineering Geology

journal homepage: www.elsevier.com/locate/enggeo

Seismic monitoring of rockfalls, slide quakes, and fissure development at the Super-Sauze mudslide, French Alps

M. Walter [a,*], C. Arnhardt [b], M. Joswig [a]

[a] Universität Stuttgart, Institute of Geophysics, Azenbergstrasse 16, 70174 Stuttgart, Germany
[b] RWTH Aachen University, Department of Engineering Geology and Hydrogeology, Lochner Strasse 4-20, 52064 Aachen, Germany

ARTICLE INFO

Article history:
Accepted 2 November 2011
Available online 13 November 2011

Keywords:
Slope dynamics
Seismic monitoring
Rockfalls
Slide quakes
Fissure development

ABSTRACT

Applying the method nanoseismic monitoring to the fast-moving mudslide in Super-Sauze (French Alps) we observed different types of seismic events caused by varying slope dynamics. We identified signals caused by rockfalls in the source area of the slope, and different types of signals, which had obviously been generated by material failure within the unstable part of the mudslide. Signal analysis and further investigations, e.g. the analysis of magnitude–frequency distribution and simultaneous measurements by nanoseismic monitoring and extensometer devices, revealed the generation of the observed seismic signals: fracture processes, i.e. slide quakes, within the unstable sediments and the development of fissures at the slope's surface. The spatial distribution of the epicenters (slide quakes), respectively the estimated source area (fissure development), correlates well with parts of the slope moving with higher velocities at the surface. Most of these signals were generated close to the in-situ crests, which are mostly covered by the mudslide material today, indicating specific dynamics in these particular slope areas.

1. Introduction

Geophysical methods like active seismics, ground penetrating radar, and geoelectrical mapping and sounding can provide information about material parameters and the stratigraphy of the subsoil (e.g. Sharma, 1997; Kearey et al., 2003). Applied to landslides, geometrical conditions and mechanical material properties can be inferred (e.g. Grandjean et al., 2007). Compared to these static, active prospecting techniques, we applied passive seismological methods in order to continuously observe the varying dynamic processes during the movement of a mudslide in the French Alps.

During a field-campaign in June 2008, we were able to detect and analyze several seismic signals caused by varying dynamic processes at the fast-moving mudslide in Super-Sauze, southern French Alps by applying the method nanoseismic monitoring (Joswig, 2008). Nanoseismic monitoring acts as a seismic 'microscope' to detect small impulsive signals in the subsurface and was first applied to map sinkholes in Israel (Wust-Bloch and Joswig, 2006). A pilot study at the Heumoes slope in the Austrian Alps was carried out in 2005, where we were able to demonstrate the existence of measurable fracture processes during the movement of soft rock landslides by the use of nanoseismic monitoring (Walter and Joswig, 2008). The existence of such signals was not expected due to the lack of brittle material deformation that would generate impulsive stress relief within such weak sediments.

Fracture processes on landslides consisting of hard rock (fragments) were monitored by e.g. Brückl and Mertl (2006) in the Austrian Alps, Spillmann et al. (2007) in the Swiss Alps and Roth et al. (2005) at the Aknes fjord in Norway. The detected fractures in these studies are probably caused by brittle deformation of the respective slope material. Compared to these studies, our work is focused on the characterization of seismic signals caused by deformations of soft rock landslide material. The terms 'fractures' and 'fracture processes' are commonly used by the seismological community and describe seismic events of low energy (microearthquakes), especially by the observation of induced seismicity (e.g. Lee and Stewart, 1981). Martel (2004) describes 'fractures' as shear failures of landslide material. Due to the assumed analogs of shear failures of landslides and stress relief along tectonic fault systems by means of strike slip deformations, Gomberg et al. (1995) suggested to establish the term of 'slide quakes' describing the fracturing or initial stress relief of slope material by means of brittle failure.

Here, we present the results of the seismic observations and characterization of varying dynamics at the mudslide in Super-Sauze by analyzing the spatio-temporal occurrence of slope deformations. Besides the observed dynamics caused by deformations of the mudslide itself (slide quakes), we recorded rockfalls occurring frequently in the source area of the mudslide, which actually lead to the enormous movement velocities of the mudslide from the mass-balancing point of view. Additionally, we observed signals caused by fissure development.

* Corresponding author.
E-mail address: Marco.Walter@geophys.uni-stuttgart.de (M. Walter).

0013-7952/$ – see front matter © 2011 Elsevier B.V. All rights reserved.
doi:10.1016/j.enggeo.2011.11.002

2. General setting and prior investigations

The mudslide at Super-Sauze is situated in the Barcelonnette Basin in the Southern French Alps, about 100 km north of Nice (Figure 1). The mudslide started to form in the 1960s and today it measures 850 m long with an elevation between 2105 m (crown) and 1740 m (toe). The unstable slope with an estimated volume of 750,000 m^3 mainly consists of heterogeneous soft Jurassic, black marls and shows an immense dynamic behavior with displacement velocities of more than 3 cm/day (Amitrano et al., 2007). The observed displacements of the mudslide vary: the highest average movements can be observed in the mid-part of the slope and decrease in toe direction to less than 2 mm/day (Figure 2). The influence of the bedrock topography on the slope stability was investigated by e.g. Malet (2003). He observed that stable buried in-situ crests at the bedrock of the mudslide directly affect the behavior of the entire slope, and that gullies between them canalize the unstable material, what causes the heterogeneous movement of the mudslide.

The mudslide at Super-Sauze has been the target of several investigations since the 1990s (Weber, 1994) in order to develop a comprehensive model for its slope instability. Geological (e.g. Weber and Herrmann, 2000), hydrological (e.g. Malet and Maquaire, 2003), geotechnical (e.g. Flageollet et al., 1996) and geophysical studies (e.g. Schmutz et al., 1999) were carried out to determine internal structures, the mechanisms, and the spectrum of influencing and interacting parameters leading to the enormous dynamic of the slope. Passive seismic investigations have been carried out on the mudslide by Amitrano et al. (2007) in order to determine the internal structures using the H/V-method (Nakamura, 1989; Parolai et al., 2002) and to record the dynamic processes. They describe how the seismic noise caused by the slope's movement correlates to displacement rates. Despite this observation, they could neither resolve single seismic events nor determine dynamic processes caused by the mudslide's movement, which lead to the increased seismic noise. That is the focus of this study by applying nanoseismic monitoring to the mudslide in Super-Sauze.

3. Data acquisition/data processing

Nanoseismic monitoring (Joswig, 2008) must be seen in a line of several approaches to extend the capabilities of seismic event location down to the level of ambient noise. Reference for these improvements is the classical concept of microseismic networks (e.g. Lee and Stewart, 1981). Seismicity is recorded by individual stations, reliable phase picking demands clear onsets and location utilizes the iterative Geiger approach. The quality control of location results is based on residual analysis of onset times. The complete opposite of microseismic networks properties is an approach recently adapted from exploration seismics, named Passive Seismic (e.g. Artman, 2006; Kochnev et al., 2007). The region of interest is covered by a large number of sensors, seismograms are stacked automatically in a grid-search method and potential events are identified by accumulation of radiated energy. No individual phase onsets can be identified, no single events can be separated out of a sequence of activity, nor can seismicity be distinguished from collocated noise sources. Depending on the number of stacked channels, signal-to-noise ratios of more than −15 dB can be handled. Between these two methods, nanoseismic monitoring offers a kind of third approach to improve the sensitivity of seismic monitoring down to background noise but to maintain the aspect of single event identification. The improvement is based on the increase in instrumental efforts by upgrading selected microseismic network sites to small arrays. Any small array (Seismic Navigating System — SNS) is comprised of a center, 3-c sensor, and a minimum of three outer instruments, 1-c seismometers in about 25–30 m distance. An even greater rate of success is due to an innovative concept for seismogram processing and event location, realized by the software HypoLine (Joswig, 2008): Any phase picking immediately results in displaying the related solution constraints, e.g. a circle for any t_S–t_P, a hyperbolae for any t_P–t_P permutation from different stations, or an array beam for related SNS phases. The quality of location is judged in a map by maximum concentration of information (circles, hyperbolae, beams or “hypolines”). The visual access to all aspects of location constraints supports a scheme of event processing where the

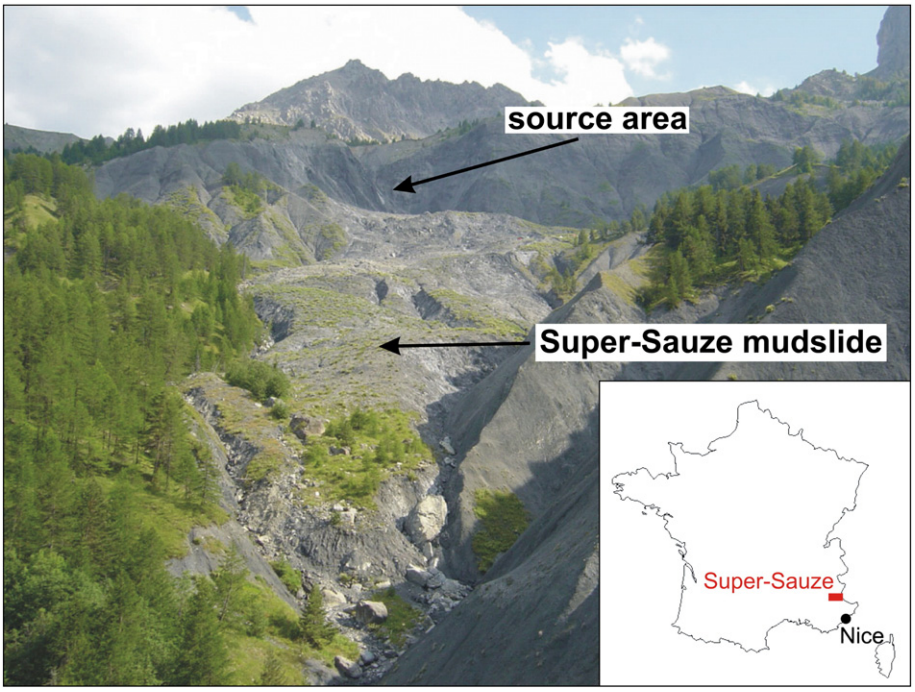

Fig. 1. Location of Super-Sauze and upward view of the mudslide and its source area in 2006.

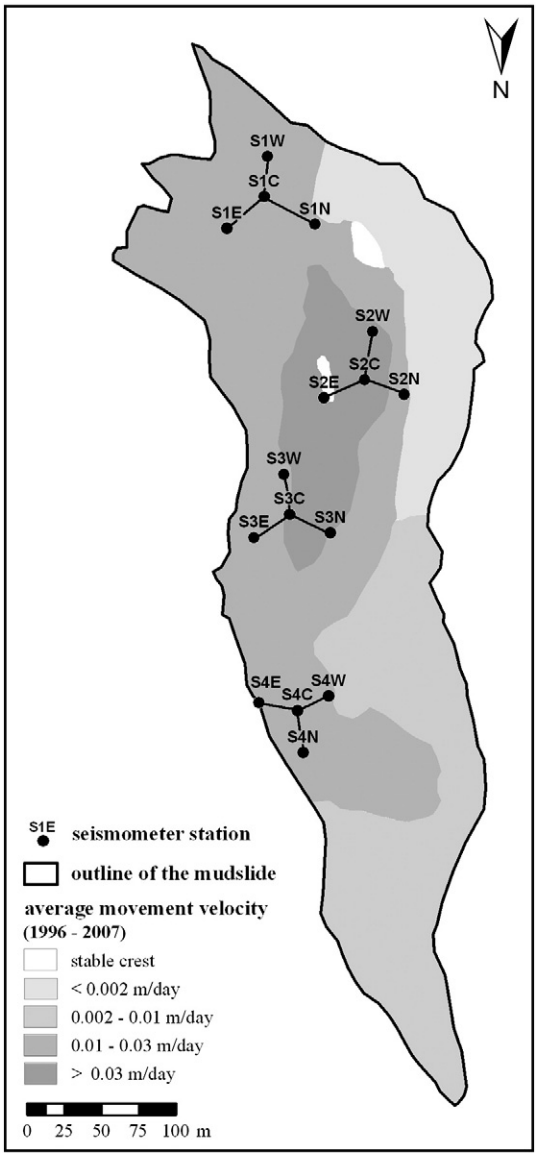

Fig. 2. Location of the installed seismometer stations (black dots) and average movement velocity of the mudslide between 1997 and 2007 determined by Amitrano et al. (2007).

analyst tests options, rates plausibility, and identifies forensic noise bursts. A comprehensive summary of all properties, advantages, and disadvantages of these three described methods is given in Table 1.

Since one finds many weak signals from unknown sources, especially when searching for small magnitude events, it is important to deal with forensic seismology (e.g. Douglas, 2007). Nanoseismic monitoring has been successively applied to the pre-collapse identification of sinkholes in Israel (Wust-Bloch and Joswig, 2006), to investigate small aftershocks after strong earthquakes (Häge and Joswig, 2009a), and to determine the microseismicity in different tectonic regimes (Häge and Joswig, 2009b). On landslides, nanoseismic monitoring has been used since 2005 on a creeping hillslope in Austria in order to map single fracture processes during its movement (Walter and Joswig, 2008).

For this study in Super-Sauze, seismic data was acquired during a 10-day campaign (July 14–24, 2008) by deploying four SNS on the mudslide (Figure 2). Data was recorded in continuous mode with a sampling rate of 400 Hz. The layout of the four SNS at the mudslide in Super-Sauze during the field campaign was chosen in order to cover seismically most of the mudslide and to concentrate on the mid-part of the slope which shows the highest dynamics at the surface (Figure 2). The raw-data was high-pass filtered above 5 Hz to eliminate anthropogenic noise sources and to increase the SNR.

Table 1
Properties of different seismic event location methods (modified after Joswig, 2008).

	Microseismic networks	Nanoseismic monitoring	Passive seismic
Signal-to-noise ratio	>+15 dB	>0 dB	>−15 dB
Phases	Clear	Questionable	Not visible
Number of stations (typical)	30 single 3c	3–5 SNS arrays	100+ array traces
Processing	pick → batch	Live update	Automated stack
Noise forensics	Optional	Essential	None
Solution info	hypo, t_0, M_L, M	hypo, t_0, M_L	Statistics
Quality control	Residuals	Plausibility	None
Master event enhancement	Possible	Possible	Not applicable

4. Calibration shot analysis

To determine an adequate underground model for the localization of possible slope dynamics, we ignited 8 calibration shots on several locations of the slope, close to our stations. The aim of the calibration shots was to determine the thickness of the unstable mudslide material as well as the velocities of the wave phases within the sediments and at the bedrock below. We observed a P- and S-wave velocity of about 600 m/s and 310 m/s within the unstable sediments, respectively. For the bedrock, we determined a P-wave velocity of about 2100 m/s and S-wave velocity of 1200 m/s.

The considerable low phase velocities as well as the higher v_P/v_S ratio of the unstable material compared to the bedrock is quite common for sedimentary bodies (e.g. Walter and Joswig, 2008) and is in accordance with prior seismic investigations at Super-Sauze (Grandjean et al., 2007). The relatively low P-wave velocity of the bedrock is also consistent with the ones observed at the mudslide in previous studies; Grandjean et al. (2007) determined a P-wave velocity between 2100 m/s and 2400 m/s. Thus, we used a layer, with a thickness of ~15 m, above half space model with the mentioned phase velocities for further event localization, if possible.

5. Signal analysis/signal classification

During the campaign in July 2008 we detected and located different types of events caused by material failure within the source area and the mudslide itself (Figure 1). The event types differed in signal duration, number of seismometer stations which recorded the signal, amplitude, frequency content and consequently in sonogram patterns. These characteristics as well as the analysis of further site-effects, like amplitude decrease, absorption and attenuation effects caused by the heterogeneity of the slope material, allowed a classification of the recorded signals (Table 2). During a pilot study of monitoring slope dynamics of soft rock landslides in the Austrian Alps, we observed only slide quake events caused by fracturing processes during its movement (Walter and Joswig, 2008). Therefore, we expected at the beginning of the field campaign to record similar seismic events, with a higher amount of them due to the stronger deformation processes at Super-Sauze. Surprisingly, we identified three different types of events on the basis of the afore-mentioned attributes,

Table 2
Classification criteria of seismic signals caused by different slope dynamics.

Classification criteria	Rockfalls	Slide quakes	Fissure development
Signal duration [s]	20–1200	2–5	2–20
Frequency content [Hz]	10–130	10–80	5–150
# of Seismometer stations [–]	8–16	4–12	4
Signal Amplitude [nm/s]	50–1500	40–200	20–7500

which are caused by varying slope dynamics: rockfalls, slide quakes and fissure development (Table 2).

6. Seismic signals of rockfalls

During the field campaign, we recorded hundreds of signals with durations between a few seconds (single event) and up to 20 min (multiple events) caused by rockfalls which occurred frequently in the source area of the mudslide (Figure 1). The signals show a 'noise band' between ~5 Hz up to ~50 Hz with broadband spikes (Figure 3). The 'noise band' is caused by the flow of fine-grained material resulting in signals comparable to those of avalanches (e.g. Suriñach et al., 2005). The spikes are caused by the impact of falling blocks, a fact that has been proven by experiments and visual observations in the field. The stronger events show maximum amplitudes (peak to peak) of 500 nm/s–1500 nm/s and were recorded on all seismometer stations; the weaker ones were recorded at the seismometer stations of only two SNS with amplitudes varying between 50 nm/s and 500 nm/s. The source area of the rockfall events was estimated by determination of the backazimuth for each SNS which recorded the signal. All these events occurred in the steep, north-facing hillsides, on the brink of the uppermost part of the mudslide. A correlation between the temporal occurrence of the rockfalls and outer influences (e.g. rainfall) wasn't observed.

Fig. 3 shows the waveforms and sonograms of a weak rockfall event that came from the north-western part of the source area, recorded on July 19, 2008 with one SNS. The signal duration is ~25 s; the amplitude scale varies between 300 and 1500 nm/s. The highest amplitudes were recorded on the station S1E. The attenuation effect and amplitude decrease is caused by the heterogeneity of the slope material.

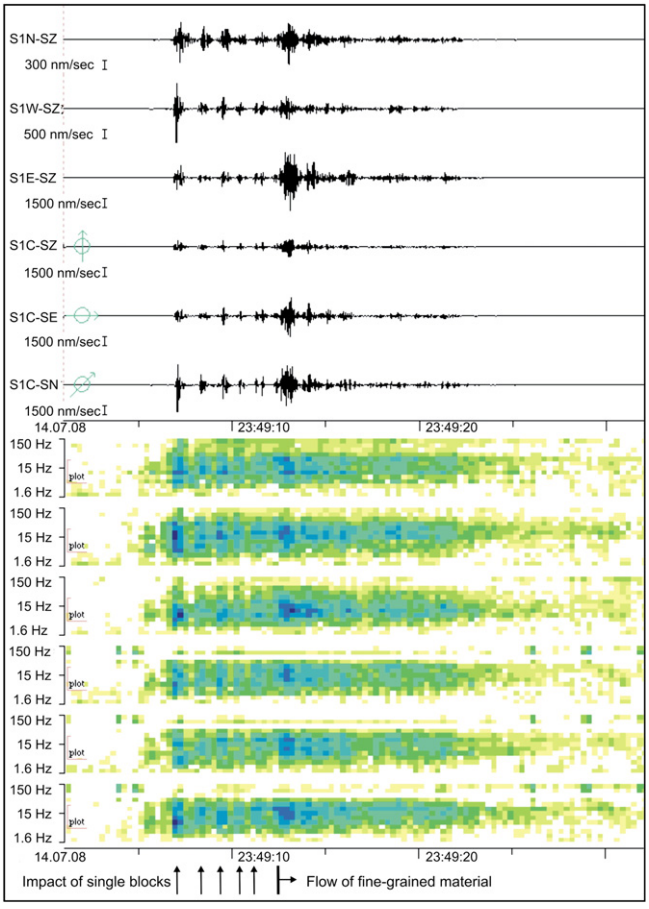

Fig. 3. Typical waveforms and sonograms of a weak rockfall event, recorded on 19th July 2008 with one SNS: the upper three traces belong to the three outer 1c-stations while the lower three traces represent the 3c-central station. The sequence of broadband spikes is caused by the impact of falling blocks while the high-frequent "noise-band" is caused by the fall of fine-grained material.

7. Seismic signals of slide quakes

During the field campaign, we detected 34 signals which show clear phase onsets (Figure 4), allowing their localization by standard seismological procedures. The duration of these events lies between 2 and 5 s, the maximum amplitude varies between 40 and 2000 nm/s (peak to peak) and the frequency content of the P-phase is concentrated between 10 and 80 Hz while the later arriving phases prevail in lower frequencies between 10 and 30 Hz. The observed events at the mudslide in Super-Sauze show remarkable similarities to the fractures we recorded at the creeping Heumoes slope in Austria (Figure 4; Walter and Joswig, 2009). For this reason we interpret these signals as results of initial stress relief, i.e. slide quakes. The signals had to be recorded on at least 2 SNS to be localizable, where the distance range for reliable detection was within some 200 m. The accuracy of localization was determined to be ~10% of the epicenter distance by the localization of the calibration shots. The emergent onset, the lack of higher frequencies above 80 Hz, and the signal incoherency indicate intense scattering caused by the high heterogeneity of slope material (Figure 4). However, the frequency content of these signals is rather similar to those of weak local earthquakes (Figure 4). Only the amplitudes and the signal lengths of these signals differ distinctly from each other. The amplitude scale of the slide quake of Fig. 4a, which was recorded in Super-Sauze, varies between 30 and 100 nm/s, while the amplitude scale of the similar event recorded at the Heumoes slope in Austria ranges between 300 and 2000 nm/s (Figure 4b) and the one of the local earthquake between 700 and 2000 nm/s (Figure 4c). These observations can be explained by the varying energy release in dependence of the epicenter distance of the different sources.

The magnitudes of the slide quakes observed at Super-Sauze vary between $-3.2 \leq M_L \leq -1.3$. They are approximately one magnitude order lower than the recorded events at the Heumoes slope in Austria where the magnitudes range between $-2.4 \leq M_L \leq -0.7$ (Walter and Joswig, 2008). The magnitudes were determined by the maximum amplitude of the S-phase. The M_L distance correction curve is based on the analysis of seismic events with short slant distances, done by Wust-Bloch and Joswig (2006), and is in accordance with other approaches (e.g. Bakun and Joyner, 1984). The magnitude variation between the events observed in Super-Sauze compared to the ones at the Heumoes slope in Austria has two reasons: First, the noise-level in Super-Sauze is about 10 dB lower, which equates to approximately one order of magnitude. Second, the lack of magnitudes $M_L > -1.0$ in Super-Sauze indicates a lower stress relief for single events, but they occur with a much higher frequency caused by the higher movement velocities compared to the Heumoes slope.

The located slide quakes are mainly clustered in the middle part of the mudslide (Figure 5). The cluster corresponds to the part of the slope showing the highest velocities at the surface. A cluster of slide quakes is located directly at the boundary between the mudslide material and one of the emerging in-situ crests in the central part of the slope (Figure 5) indicating higher deformation processes close to the crest. Not displayed in Fig. 5 are three events which were localized in the south, outside of the slope catchments. They were probably generated by material failure in the hard rock mass in the source area of the mudslide (Walter and Joswig, 2009). As the event depth could not be evaluated due to the sparse station distribution, it is impossible to estimate at which depth and along which material interface the source processes took place exactly.

Fig. 6 displays the localized slide quakes mapped on an aerial picture from 1957 before the mudslide occurred (by courtesy of Institut

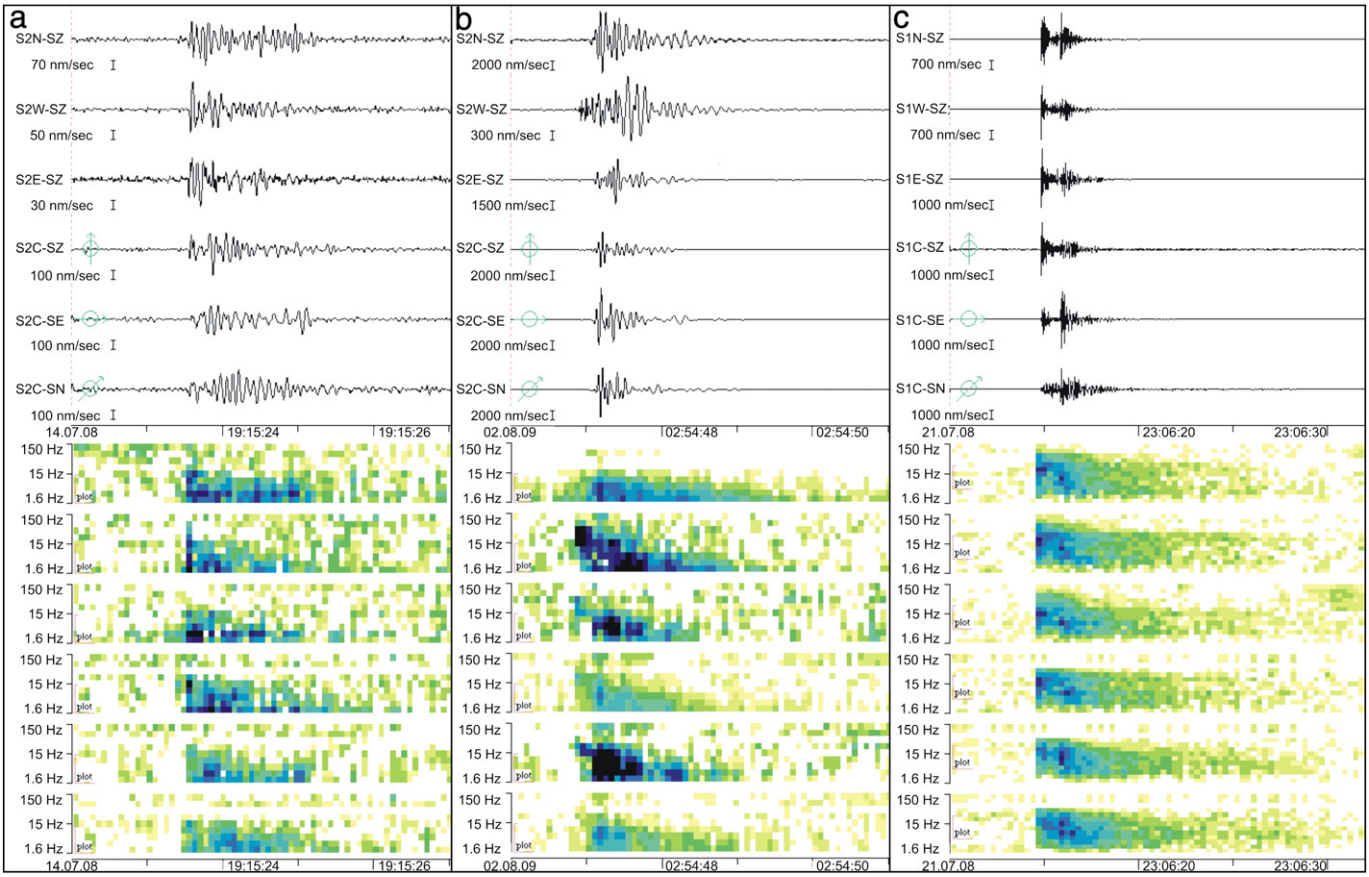

Fig. 4. Typical waveforms and sonograms of slide quakes and local earthquakes recorded with one single SNS: the upper three traces belong to the three outer 1c-stations while the lower three traces represent the 3c-central station. (a) slide quake $M_L = -2.2$ in ~120 m distance in Super-Sauze, recorded with SNS 2 (Figure 2); (b) slide quake $M_L = -1.4$ in ~180 m distance on the creeping Heumoes landslide, Austria; (c) local earthquake $M_L = 2.0$ in ~15 km distance in Super-Sauze, recorded with SNS 2 (Figure 2). Note the different time and amplitude scales.

Geographique National, Campaign F3139–3639). Most of the epicenters are located on top of the in-situ crests or in the vicinity of them, today hidden by the mudslide material. This observation supports prior investigations of a direct interaction between the mudslide's behavior and the topography of the bedrock below (e.g. Malet, 2003).

The temporal occurrence of recorded slide quakes, their magnitudes and the rain intensity during the field campaign is displayed in Fig. 7. It seems that the mudslide moves more or less continuously, indicated by the well-distributed temporal occurrence of the signals all over the measurement period. Note that a cluster of events with the highest magnitudes occurred just a few hours after the rain event on July 21, 2008. Compared to our seismic investigations at the Heumoes slope in Austria (Walter and Joswig, 2008), a direct coupling of rainfall and stress relief in the mudslide's material couldn't be observed due to the low precipitation during the field campaign resulting in a minor change of the state of stress of the mudslide.

8. Frequency–magnitude relation of slide quakes

In the time since the crucial contribution made by C. Richter in 1935 concerning the concept of earthquake magnitude, it has been revealed that earthquakes are not uniformly distributed in time, space and magnitude. The empirical Gutenberg–Richter law $\log_{10} N = a - bM$ defines the distribution of earthquakes with respect to the magnitude. N is the cumulative number of earthquakes with magnitude M or greater which occur in a given area. The constant a defines the seismic activity and b is a tectonic parameter describing the relative abundance of large to smaller events (Ishimoto and Iida, 1939; Gutenberg and Richter, 1942). The b-value represents properties of the seismic medium, like stress and/or material conditions in the focal area, and ranges between 0.6 and 1.4 for most of the tectonic regimes. Globally it averages around 1. The Gutenberg–Richter relation has also been studied during rock deformation experiments in laboratories (e.g. Scholz, 1968). Scholz observed that the frequency–magnitude relation for events which accompanied frictional sliding and deformation of a ductile rock have a much higher b-value ($\sim b > 1$) than that observed in brittle rock ($\sim b < 1$).

Statistics related to the Gutenberg–Richter power law should be drawn from a sufficient number of events. Schorlemmer and Wiemer (2004) propose 50–100 events for reliable b-value estimation. On the other hand, Neunhöfer and Hemmann (2005) expect only a small b-value error for a calculation with ≥10 events. The b-value of the recorded slide quakes in Super-Sauze was calculated with 22 events with magnitudes $M_L \geq M_C$, where M_C is the magnitude of completeness or the detection threshold during the measurement period. The error of magnitude determination was estimated to be +/−0.1. Hence the magnitude of completeness is $M_C = -2.6 +/ -0.1$ (Figure 8). The cumulative and the incremental number of slide quakes as well as the b-value are illustrated in the frequency–magnitude distribution in Fig. 8. The b-value was calculated to be $0.84 +/- 0.18$; the standard error was estimated after Utsu (1965) with $b_{err} \approx b/\sqrt{N}$, where N is the number of events with $M_L \geq M_C$.

Two results regarding the frequency–magnitude analysis of the slide quakes in Super-Sauze are notable: First, the frequency–magnitude distribution of the slide quakes caused by slope deformations fits to

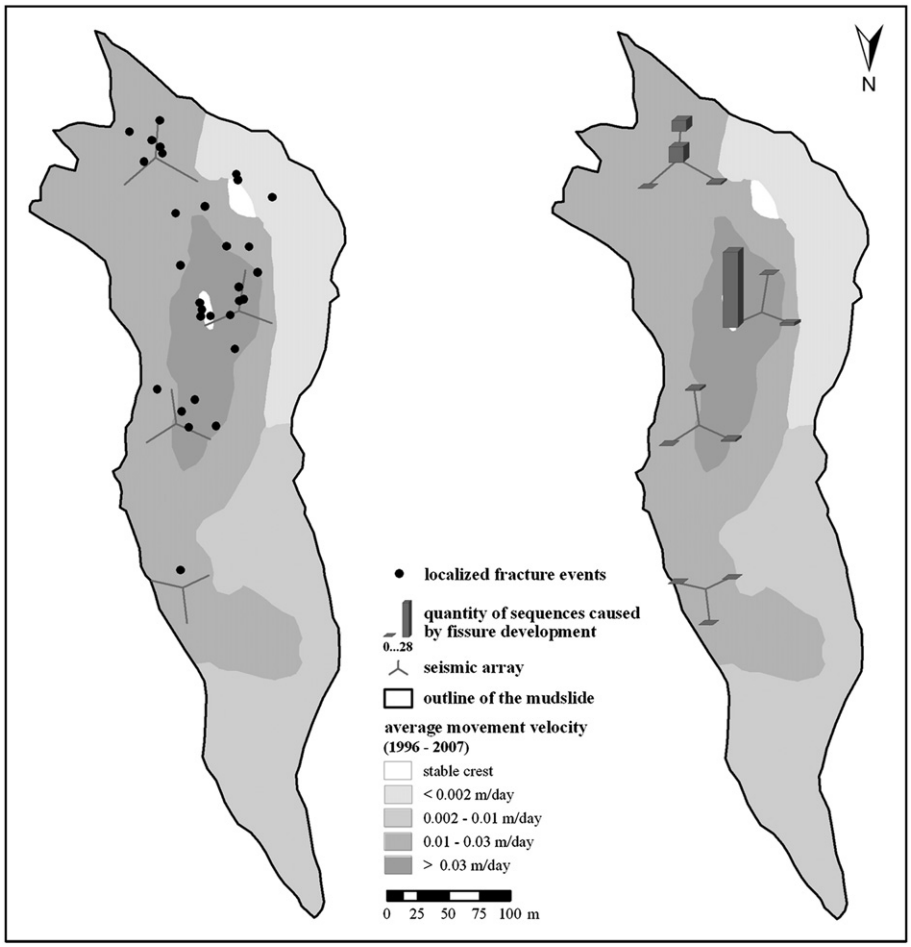

Fig. 5. Epicenters of the slide quakes (left) and quantity of sequences caused by superficial fissure development (right) mapped on the average movement velocity of the mudslide (1997–2007) determined by Amitrano et al. (2007).

the empirical Gutenberg–Richter power law. Second, the calculated b-value of $b = 0.84 +/- 0.18$ is in accordance with b-values ($\sim b < 1$) observed during brittle rock deformations by Scholz (1968).

However, the mudslide material consists of weak sediments, whose deformations depend on the water saturation. Maquaire et al. (2003) carried out ring shear tests with the slope material in order to obtain information on the strength and the effects of moisture content on the effective cohesion and effective angle of friction. They determined the deformations of the slope material in dependence of its water content. With up to 27–28% water content, the material deforms in a brittle manner, while a higher water content leads to flow deformations. These material properties can be observed in the field when the material dries out in summertime. Then the surface of the slope shows lots of fissures, which reach a maximum depth of around 1 m; the material below is completely water saturated. We can therefore assume that these observed slide quakes are caused by initial stress relief, or brittle failure processes, within the first meter of the slope material. Brittle material deformation is actually needed for both: initial stress relief, slide quakes respectively, and fissure development at the mudslide's surface.

9. Seismic signals of fissure development

Besides seismic signals caused by rockfalls and slide quakes, we recorded and identified 44 signals showing significant differences (Table 2). The increased sensitivity at the mudslide in Super-Sauze compared to our seismic measurements at the Heumoes slope in Austria resulted in the detection of signals caused by the movement of the slope, which lay barely above the low, ambient noise level. For this reason, these events weren't observed at the Heumoes slope and weren't expected at the mudslide in Super-Sauze. The duration of these events, which were only recorded at one single SNS, varied between 2 and 20 s. Compared to the other event types, the signal energy prevailed at higher frequencies: up to 150 Hz at the closest station in the array (Figure 9). Due to the heterogeneity of the slope material, we saw enormous attenuation effects within one single SNS; the signal amplitude decreased about 30 times within one single SNS at the same time (Figure 9).

Similar to the rockfall events, no wave phases could be identified in the signals, which prevented their localization by standard seismological procedures. Therefore we could only estimate the source area, which is for obvious reasons, in the vicinity of the closest station with the highest recorded amplitude. Fig. 5 shows the seismometer stations and the quantity of the recorded events generated near the stations during the entire field campaign. Like the slide quake locations, most of these events occurred in the central part of the slope. Similar to the spatial distribution of the localized fracture processes, the source area of the majority of them was estimated to be close to the station S2E (Figure 2), at the boundary of the slope material and one of the emerging in-situ crests (Figure 5). This observation proves prior assumptions of specific dynamics close to these (emerging) in-situ crests and lateral boundaries of the mudslide (e.g. Malet, 2003).

A first model of the generation of these seismic signals interprets these events as a result of 'scratching' and 'grinding' sequences of the mudslide material against the (emerging) in-situ crests (Walter and Joswig, 2009). The joint analysis by nanoseismic monitoring and UAV (Unmanned Aerial Vehicle) based remote sensing (Niethammer et al.,

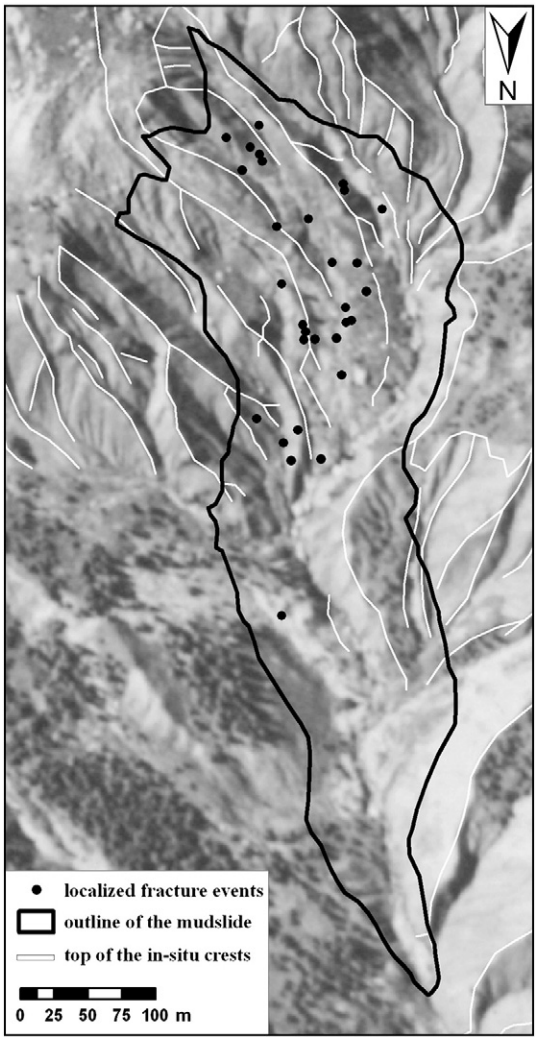

Fig. 6. Epicenters of the located slide quakes mapped on an airborne picture from 1956, courtesy of IGN (Institut Geographique National, Campaign F3139–3639). Highlighted are the tops of the in-situ crests of the bedrock's topography.

2009; Walter et al., 2009; Niethammer et al., in press) reveals the generation of these signals by fissure development on the mudslide's surface. The high-resolution pictures of the mudslide in Super-Sauze by UAV-based remote sensing show specific deformations of the mudslide material at (emerging) in-situ crests and lateral boundaries resulting in particular fissure patterns at the surface (Niethammer et al., in press).

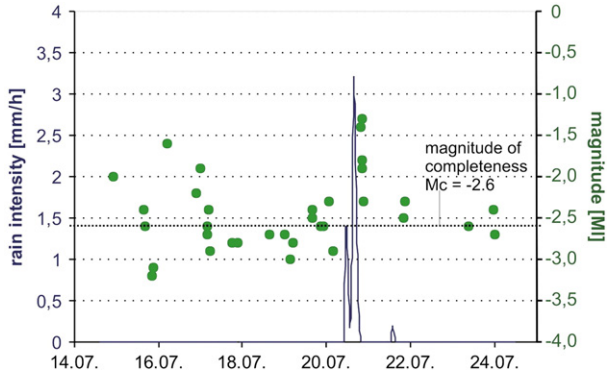

Fig. 7. Rain intensity (blue) and temporal occurrence of the slide quakes with their magnitudes M_L (green) during the field campaign July 14–24, 2008. The dashed line marks the magnitude of completeness $M_C = -2.6$ (Figure 8).

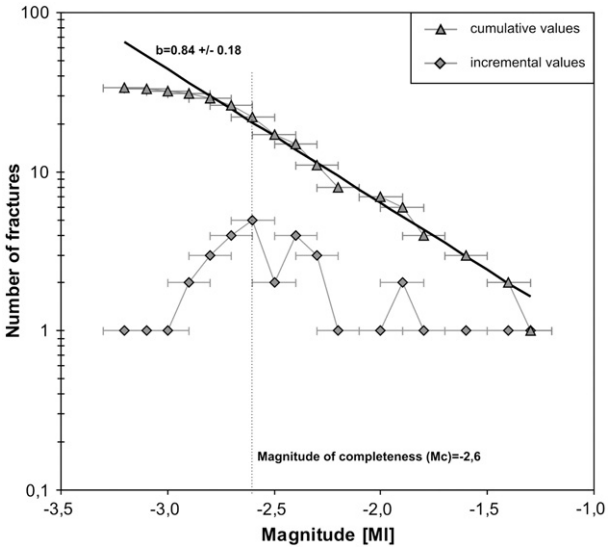

Fig. 8. Frequency–magnitude distribution and b-value of the recorded slide quakes in July 2008 at the mudslide in Super-Sauze. The determined magnitude of completeness (M_C) is shown with the black dashed line. The horizontal error bars mark the uncertainty of magnitude determination of +/−0.1.

The assumption of the generation of seismic signals caused by fissure development was supported by simultaneous in-situ measurements of fissure development applying nanoseismic monitoring and

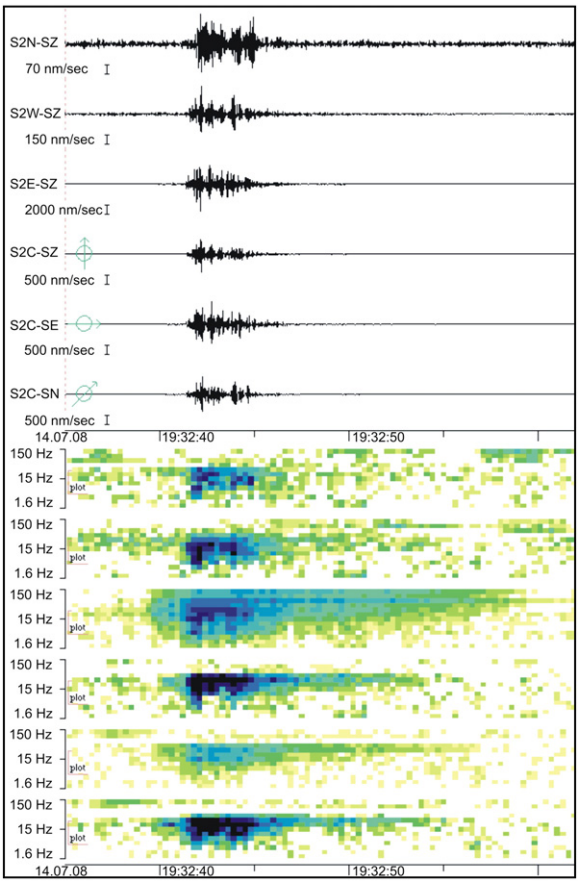

Fig. 9. Typical waveforms and sonograms of an event caused by fissure development at the mudslide's surface (see text), recorded with SNS 2 (Figure 2): the upper three traces belong to the three outer 1c-stations while the lower three traces represent the 3c-central station. Note the different amplitude scales, signal duration and frequency content.

measurements by extensometers from July 20–24, 2009. The extensometer was installed above an existing fissure at the lateral boundary of the mudslide; one 1c-seismometer station was installed below, directly in the fissure (Figure 10).

The installed extensometer, also called draw wire displacement transducer, was integrated in a Wireless Sensor Network (WSN) and was used to monitor the opening and widening of fissures at the mudslide. The whole system is part of a research project at the Department of Engineering Geology and Hydrogeology (LIH) of the RTWH-Aachen University, Germany and deals with the development of a prototypic Alarm- and Early Warning System (EWS) for different types of landslides using modern wireless sensor networks and different measuring devices (Arnhardt et al., 2010). The position sensor measures linear movements along a highly flexible and calibrated measuring cable or draw wire. The resolution of the sensor was 0.1 mm and changes of 0.1 mm in length and higher could be detected with high precision. For movement detection the position sensor itself was mounted on one side of the fissure, while the other end of the wire was fixed to a ground nail on the other side (Figure 10). The Sensor was connected with a sensor node (radio module) of the WSN that allowed the data transmission via radio signal to a collection point (gateway; Fernandez-Steeger et al., 2009).

Fig. 11 illustrates the results of geotechnical measurements (groundwater level, GPS device), the extensometer measurements as well as the cumulative number of seismic events generated at the same place from July 13–25, 2009. The groundwater level (GWL) shows variations of ~13 cm during these 13 days (Figure 11a). Remarkable are three abrupt raises of ~3–6 cm between July 21–23, 2009. During the measurement period, we detected additional displacements of ~5 cm with a permanent GPS device. Besides the continuous movement of the mudslide, the abrupt increase of the GWL led to higher planimetric displacements at the surface within a time interval of a few hours compared to the change of the GWL (Figure 11b). We observed planimetric displacements of ~2 cm within these three days. The extensometer detected displacements, or fissure openings, of ~15 mm from July 21–24, 2009 (Figure 11c). Distinguishable again are the three episodes of higher rates of fissure opening which directly correspond to the three episodes of higher displacements of the entire mudslide measured by the GPS device. The cumulative number of seismic events caused by fissure opening located at the seismometer station close by the extensometer (Figure 10) is given in Fig. 11d. The temporal occurrence of the seismic events correlates well with the measured displacements of the entire mudslide (GPS device) as well as with the rate of fissure opening recorded by the extensometer. Despite that, from July 17–20, 2009, we observed quite a low number of seismic events. That was probably caused by the linear decrease of the GWL, which on the other hand led to displacements of only ~6 mm within these 4 days, less than a fourth of displacements per day observed during the abrupt increasing GWL from July 21–24, 2009.

Generally, the simultaneous observations in July 2009 prove our model that these seismic events are generated by fissure development at the surface of the mudslide. An increase of the GWL lead to higher deformation rates of the entire mudslide (Malet and Maquaire, 2003) as well as to higher rates of fissure opening. The higher rates of fissure opening correlate well with the temporal occurrence of these seismic events. Additionally, by chance, one of our seismometers dropped into a newly opened fissure on July 22, 2008, producing a perfect reference pulse. In the last few hours before that reference pulse, we had observed four of those events close by, indicating recent fissure development.

Similarly to the slide quakes, a brittle deformation of the slope material is needed to generate measurable seismic signals caused by fissure development. But compared to the slide quakes the energy release is much lower and confined to a smaller area than these events and can only be recorded within one single SNS. The fissure development is confined to a maximum depth of ~1 m, where the water saturation of the sliding material varies seasonally. In summertime, the material dries out and similarly to the slide quakes, the necessary material properties (dependent on the water saturation) of brittle failure can be observed. On the other hand, the displacements measured by the GPS device are caused by a viscous or ductile movement of the entire slope, while at the same time the fissure opening observed by the extensometer is caused by brittle deformation. For further investigations of possible source processes, we compared the observed signals caused by fissure development with the ones caused by rockfalls. One possible hypothesis is that the impact of

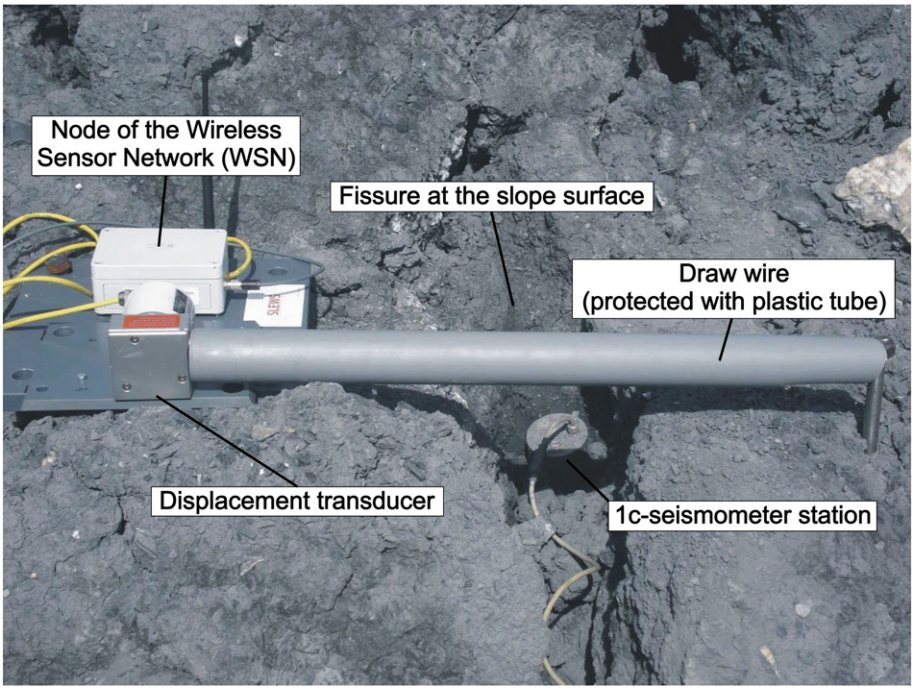

Fig. 10. General set-up to observe fissure development applying nanoseismic monitoring and extensometer measurements.

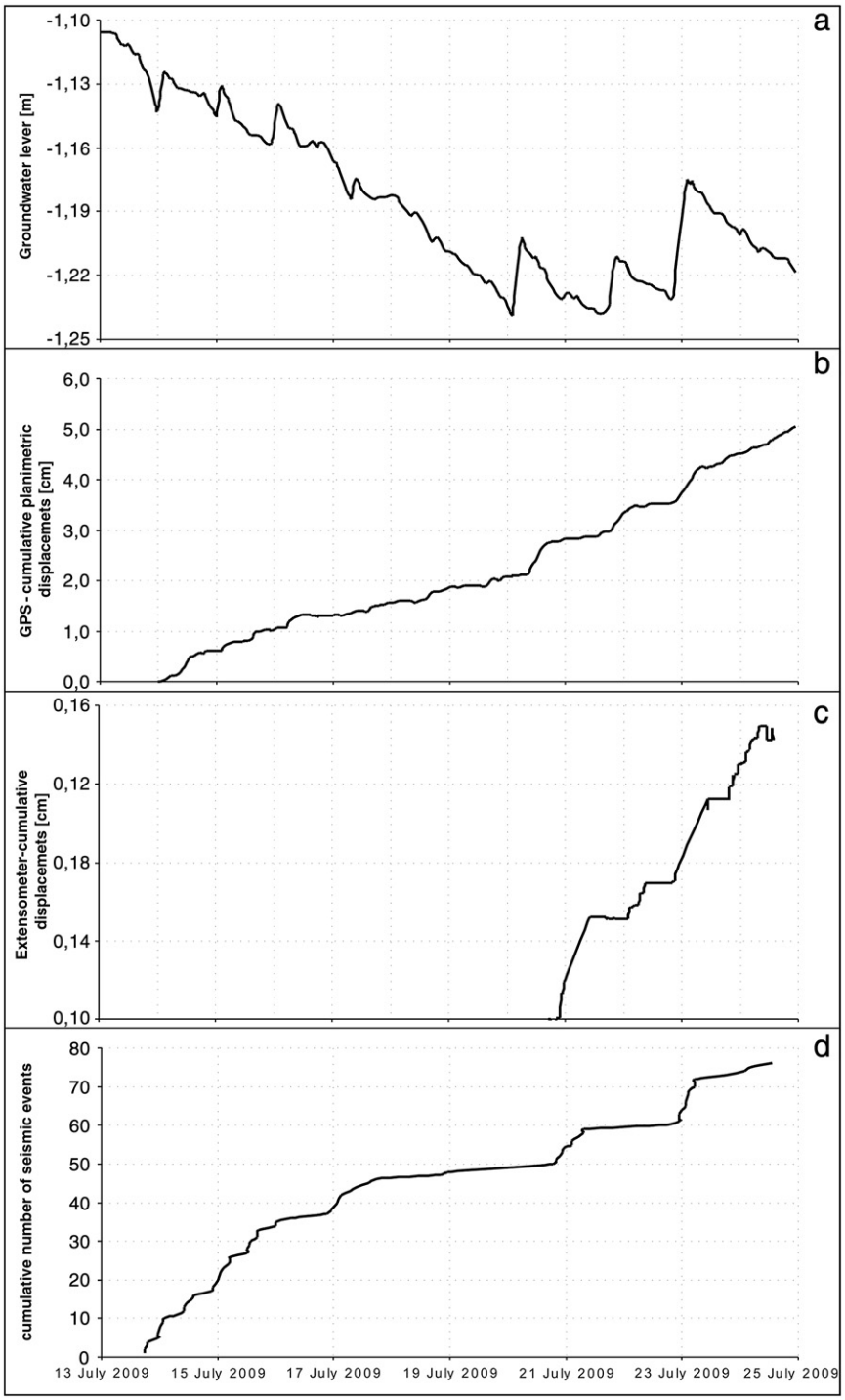

Fig. 11. (a) Groundwater level from July 13–25, 2009; (b) cumulative planimetric displacements measured with a GPS device from July 13–25, 2009; (c) cumulative displacements measured with extensometer from July 21–25, 2009; (d) cumulative number of seismic events caused by fissure development from July 13–25, 2009.

fine grained material with the size up to a few cm in an existing fissure could generate the observed signals. These processes were also visually observed in the field. That model would explain the long signal duration up to ~20 s, the high amplitude at the seismometer station nearby, the enormous attenuation effects and the confinement to a small area compared to the fracture events (Table 2). Indeed, the sonogram and seismogram patterns of these events show remarkable similarities to the rockfall events. Fig. 12 shows the comparison of waveforms and sonograms of the rockfall event of Fig. 3 and the event caused by fissure development of Fig. 9. To compare the dominant frequencies of both signals, the rockfall signal was resampled down to 200 Hz.

In both cases the signal shows an increasing frequency as opposed to the signals caused by slide quakes (and local earthquakes; Figure 4), where the frequency decreases. The signal initiated by fissure development is more a sequence than a discrete seismic event like the slide quake events. We visually observed in the field that the broadband spikes represent the impact of material particles >~1 cm, whereas the high frequent “tail” of the signal is caused by the fall of fine-grained material <~1 cm. The fact that the signals of

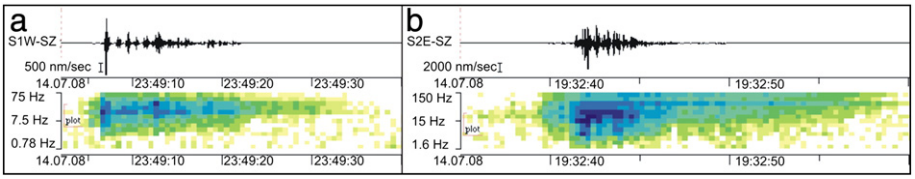

Fig. 12. Comparison of waveforms and sonograms caused by rockfalls and fissure development. (a) Rockfall event of Fig. 3 recorded by station SNW (Figure 2); (b) Signal of fissure development of Fig. 9 recorded by station S2E (Figure 2). Note the different amplitude, frequency and time scales.

fissure development are higher frequent than the ones of rockfalls is due to the much smaller distance of the seismometer stations to the source, which results in lower attenuation effects by the heterogeneous slope material.

10. Conclusions and discussion

By applying the method nanoseismic monitoring (Joswig, 2008; Table 1), we were able to detect and partially locate distinct types of events caused by the dynamics at the Super-Sauze mudslide. Waveform and sonogram analysis were applied to discriminate the event types (Table 2). We identified signals caused by rockfalls, slide quakes and fissure development. The rockfall signals show remarkable similarities to those of avalanches (e.g. Suriñach et al., 2005). The 'noise band' with a frequency range between ~5 Hz and ~50 Hz is caused by fine-grained material while the broadband spikes represent the impact of blocks, which has been proved by experiments and visual observations in the field (Figure 3). The source area of the rockfalls is estimated to be at the uppermost part of the slope, where rockfalls with particles of varying size occur frequently (Figure 1).

Beside rockfalls, we recorded 34 slide quake events with magnitudes between $-3.2 \leq M_L \leq -1.3$ which show significant similarities to the ones we observed at the creeping Heumoes slope in the Austrian Alps (Figure 4). The spatial distribution of the localized slide quakes correlates quite well with parts of the slope showing the highest movement velocities (Figure 5). The highest magnitudes of these events were observed a few hours after a rainfall event on July 21, 2008 (Figure 7). Besides that, the temporal occurrence of these slide quakes was more or less uniformly distributed over the whole measurement period. The analysis of the magnitude–frequency distribution shows that the slide quake events follow the empirical Gutenberg–Richter relationship, with a *b*-value of $b = 0.84 +/- 0.18$ for events with magnitudes higher than the magnitude of completeness $M_C = -2.6 +/- 0.1$ (Figure 8). The calculated *b*-value is in accordance with *b*-values ($\sim b < 1$) which were observed during brittle rock deformations by Scholz (1968). The magnitude of completeness has to be considered regarding the spatio-temporal occurrence of the slide quakes, but doesn't influence the observations and interpretation in general.

Additionally, we identified seismic signals caused by fissure development at the surface of the mudslide. The signals, which were only recorded with one single SNS, show an enormous amplitude decrease and attenuation of high frequencies within a few meters (Figure 9). The majority of these events are generated, comparable with the slide quake locations, close to the emerging in-situ crest of the slope (Figure 5). Two, completely different observations and analyses regarding possible source processes were made. First, simultaneous measurements of fissure development by nanoseismic monitoring and extensometer devices in July 2009 (Figure 10) show that these signals could be generated by fissure opening. The temporal occurrence of the seismic events correlates well with the measured opening of an existing fissure (Figure 11). Second, sonograms of rockfall events show remarkable similarities to those of events generated by fissure development, indicating comparable processes on different scales (Figure 12). In contrast to the first observation, the impact of fine-grained material in an existing fissure would describe processes of fissure closing, what contradicts to fissure opening processes as possible source mechanisms. Additionally, a mechanical model describing the brittle deformation of fissures and viscous or ductile deformation of the entire slope at the same time cannot be derived easily. The comprehensive analysis of the geomechanical processes which generate the observed signals of fissure deformations mark one of the main tasks in future.

Stress relief within weak sediment material can be generated depending on its water saturation. Shear strength analysis of the material of the mudslide at Super-Sauze, depending on its water saturation shows the highest values between 12 and 15% water content, up to 27–28% water content the material deforms in a brittle manner generally (Malet, 2003). These values are consistent with those of the first few meters beneath the surface of the slope. Below, the material is more or less water saturated. As a brittle material deformation is needed for both, impulsive stress relief and the generation of fissures, we presume that the slide quakes as well as the signals caused by fissure development are generated close to or directly at the surface, respectively.

The fact that we located most of the slide quakes as well as the majority of events caused by fissure development directly at the boundary between the sliding material and one of the emerging in-situ crests suggests the possibility of higher stress relief in general at that boundary. To prove this assumption, we overlaid the location of all these events with an airborne picture taken in 1956, before the mudslide occurred (Figure 6). Most of the epicenters are located on top of the in-situ crests, today hidden by the mudslide material. Specific fissure patterns at the mudslide's surface in that area observed by UAV-based remote sensing prove the observation of differing dynamics in that area (Walter et al., 2009; Niethammer et al., in press).

In close collaboration with colleagues from the OMIV-project (Observatoire Multidisciplinaire des Instabilités de Versants), a hydrological model will be developed in the future in order to verify the spatio-temporal occurrence of seismic signals and the hydrological properties of the mudslide's material. The joint investigations of the mudslide in Super-Sauze by nanoseismic monitoring and UAV-based remote sensing will be extended, focussing on spatially limited areas of the slope, e.g. focussing on the emerging in-situ crest where specific deformations take place. A permanent seismic network was installed in summer 2009 on the mudslide by colleagues from the University of Strasbourg in order to prove our first observations and to investigate the spatio-temporal occurrence of the seismic events by long-term observations.

Acknowledgments

The authors are especially grateful to Jean-Philippe Malet (school and observatory of earth sciences, University of Strasbourg, France) for both providing several datasets (Figure 11) and pictures (Figure 1) and for the very helpful discussions and improvements. We thank Guillaume Daniel as well as an anonymous reviewer for their help to improve the manuscript. We are thankful to all the colleagues who joined and supported us at the mudslide in Super-Sauze in July 2008. This research was performed within the research

unit “Natural Slopes – Coupling of Flow and Deformation Processes for Modeling the Movement of Natural Slopes” which is funded by the DFG (German Research Foundation).

References

Amitrano, D., Gaffet, S., Malet, J.-P., Maquaire, O., 2007. Understanding mudslides through micro-seismic monitoring: the Super-Sauze (South-East French Alps) case study. Bulletin de la Société Géologique de France 178 (2), 149–157.

Arnhardt, C., Fernandez-Steeger, T.M., Azzam, R., 2010. Sensorfusion in an ad-hoc Multi-hop Sensor network for real-time monitoring of landslides endangering human infrastructures. GEOTECHNOLOGIEN Science Report 15. Early Warning Systems for Transportation Infrastructures, pp. 38–49.

Artman, B., 2006. Imaging passice seismic data. Geophysics 71, 177–187.

Bakun, W.H., Joyner, W.B., 1984. The ML scale in Central California. BSSA 74, 1827–1843.

Brückl, E., Mertl, S., 2006. Seismic monitoring of deep-seated mass movements. Proceedings of INTERPRAEVENT International Symposium “Disaster Mitigation of Debris Flows, Slope Failures and Landslides.”. Universal Academy Press, Inc., Tokyo, Japan, pp. 571–580.

Douglas, A., 2007. Forensic seismology revisited. Surveys in Geophysics 28, 1–31.

Fernandez-Steeger, T.M., Arnhardt, C., Walter, K., Haß, S., Niemeyer, F., Nakaten, B., Homfeld, S.D., Asch, K., Azzam, R., Bill, R., Ritter, H., 2009. SLEWS — a prototype system for flexible real time monitoring of landslides using an open spatial data infrastructure and wireless sensor networks. GEOTECHNOLOGIEN Science Report 13. Early Warning Systems in Earth Management, pp. 3–15.

Flageollet, J.C., Maquaire, O., Weber, D., 1996. Geotechnical investigations into the Super-Sauze landslide. Geomorphological and hydrogeological results. Workshop: ‘Landslides-Flash floods’ Barcelonnette-Vaison la Romaine. CERG, European Council, pp. 30–38.

Gomberg, J., Bodin, P., Savage, W., Jackson, M.E., 1995. Landslide faults and tectonic faults, analogs?: The Slumgullion earthflow, Colorado. Geology 23 (1), 41–44.

Grandjean, G., Malet, J.-P., Bitri, A., Méric, O., 2007. Geophysical data fusion by fuzzy logic for imaging the mechanical behaviour of mudslides. Bulletin de la Societe Geologique de France 178 (2), 127–136.

Gutenberg, B., Richter, C.F., 1942. Earthquake magnitude, intensity, energy and acceleration. BSSA 32, 163–191.

Häge, M., Joswig, M., 2009a. Spatiotemporal distribution of aftershocks of the 2004 December 5 $M_L = 5.4$ Waldkirch (Germany) earthquake. Geophysical Journal International 178, 1523–1532.

Häge, M., Joswig, M., 2009b. Spatiotemporal characterization of interswarm period seismicity in the focal area Nový Kostel (West Bohemia/Vogtland) by a short-term microseismic study. Geophysical Journal International 179, 1071–1079.

Ishimoto, M., Iida, K., 1939. Observations sur les seismes enregistres par le microsismographe construit dernierement (1). Bulletin of the Earthquake Research Institute, University of Tokyo 17, 443–478.

Joswig, M., 2008. Nanoseismic Monitoring fills the gap between microseismic networks and passive seismic. First Break 26, 121–128.

Kearey, P., Brooks, M., Hill, I., 2003. An Introduction to Geophysical Exploration, third ed. Blackwell Publishing. 262 pp.

Kochnev, V.A., Goz, I.V., Polyakov, V.S., Murtayev, I.S., Savin, V.G., Zommer, B.K., Bryksin, I.V., 2007. Imaging hydraulic fracture zones from surface passive seismic data. First Break 25, 77–80.

Lee, W.H.K., Stewart, S.W., 1981. Principles and applications of microseismic networks. Advances in Geophysics. Suppl. 2Academic Press, London.

Malet, J.-P., 2003. Les glissements de type écoulement dans les marnes noires des Alpes du Sud. Morphologie, fonctionnement et modélisation hydro-mécanique. Phd thesis, Université Louis Pasteur, Strasbourg: 364 p.

Malet, J.-P., Maquaire, O., 2003. Hydrological behaviour of earthflows developed in clay-shales: investigation, concept and modeling. In: Picarelli, L. (Ed.), The Occurrence and Mechanisms of Flows in Natural Slopes and Earthfills. Patron Editore, Bologna, pp. 175–193.

Maquaire, O., Malet, J.-P., Remaître, A., Locat, J., Klotz, S., Guillon, J., 2003. Instability conditions of marly hillslopes: towards landsliding or gullying? The case of the Barcelonnette Basin, South East France. Engineering Geology 70, 109–130.

Martel, S.J., 2004. Mechanics of landslide initiation as a shear fracture phenomenon. Marine Geology 203, 319–339.

Nakamura, Y., 1989. A method for dynamic characteristics estimations of subsurface using microtremors on the ground surface. Quarterly Report of Railway Technical Research Institute (RTRI), Japan 30, 25–33.

Neunhöfer, H., Hemmann, A., 2005. Earthquake swarms in the Vogtland/Western Bohemia region: spatial distribution and magnitude-frequency distribution as an indication of the genesis of swarms? Journal of Geodynamics 39, 361–385.

Niethammer, U., Rothmund, S., Joswig, M., 2009. UAV-based remote sensing of the slow-moving landslide Super-Sauze. In: Malet, J.-P., Remaître, A., Boogard, T. (Eds.), Proceedings of the International Conference on Landslide Processes: From Geomorpholgic Mapping to Dynamic Modelling. CERG Editions, Strasbourg, pp. 69–74.

Niethammer, U., James, M.R., Rothmund, S., Travelletti, J., Joswig, M., in press. UAV-based remote sensing of the Super-Sauze landslide: Evaluation and results. Eng. Geol. doi:10.1016/j.enggeo.2011.03.012.

Parolai, S., Bormann, P., Milkereit, C., 2002. New relationship between V_S, thickness of sediments, and resonance frequency calculated by the H/V ratio of seismic noise for the Cologne area (Germany). BSSA 92 (6), 2521–2527.

Roth, M., Dietrich, M., Blikra, L.H., Lecomte, I., 2005. Seismic monitoring of the unstable rock slope at Åknes, Norway. NORSAR, Report for the International Centre for Geohazards.

Schmutz, M., Guérin, R., Maquaire, O., Descloîtres, M., Schott, J.-J., Albouy, Y., 1999. Contribution of a combined TDEM (Time-Domain Electromagnetism) and electrical survey to the investigation of the super sauze flowslide internal structure. Comptes Rendus de l'Academie de Sciences - Serie IIa: Sciences de la Terre et des Planetes 328 (12), 797–800.

Scholz, C.H., 1968. The frequency-magnitude relation of microfracturing in rock and its relation to earthquakes. BSSA 58 (1), 399–415.

Schorlemmer, D., Wiemer, S., 2004. Earthquake statistics at Parkfield: 1. Stationarity of b values. Journal of Geophysical Research 109, B12308. doi:10.1029/2004JB003235.

Sharma, P.V., 1997. Environmental and Engineering Geophysics. Cambridge University Press, Cambridge, UK. 475 pp.

Spillmann, T., Maurer, H., Green, A.G., Heincke, B., Willenberg, H., Husen, S., 2007. Microseismic investigations of an unsTable mountain slope in the Swiss Alps. Journal of Geophysical Research 112, B07301.

Suriñach, E., Vilajosana, I., Khazaradze, G., Biescas, B., Furdada, G., Vilaplana, J.M., 2005. Seismic detection and characterization of landslides and other mass movements. Natural Hazards and Earth System Sciences 5, 791–798.

Utsu, T., 1965. A method for determining the value of b in the formula $\log N = a - bM$ showing the magnitude–frequency relation for earthquakes. Geophysical Bulletin Hokkaido University 13, 99–103.

Walter, M., Joswig, M., 2008. Seismic monitoring of fracture processes generated by a creeping landslide in the Vorarlberg Alps. First Break 26, 131–135.

Walter, M., Joswig, M., 2009. Seismic characterization of slope dynamics caused by softrock-landslides: the Super-Sauze case study. In: Malet, J.-P., Remaître, A., Boogard, T. (Eds.), Proceedings of the International Conference on Landslide Processes: From Geomorphologic Mapping to Dynamic Modelling. CERG Editions, Strasbourg, pp. 215–220.

Walter, M., Niethammer, U., Rothmund, S., Joswig, M., 2009. Joint analysis of the Super-Sauze (French Alps) mudslide by nanoseismic monitoring and UAV-based remote sensing. First Break 27 (8), 75–82.

Weber, D., 1994. Research into earth movements in the Barcelonnette basin. In: Casale, R., Fantechi, R., Flageollet, J.C. (Eds.), Temporal Occurrence and Forecasting of Landslides in the European Community, Final report, Volume I., Contract EPOCH. European Comission, pp. 321–336.

Weber, D., Herrmann, A., 2000. Reconstitution de l'évolution géomorphologique de versants insTables par photogrammétrie numérique: l'exemple du glissement de terrain de Super-Sauze (Alpes-de-Haute-Provence, France). Bulletin de la Société Géologique de France 171, 637–648.

Wust-Bloch, H., Joswig, M., 2006. Pre-collapse identification of sinkholes in unconsolidated media at Dead Sea area by “nanoseismic monitoring” (graphical jackknife location of weak sources by few, low-SNR records). Geophysical Journal International 167, 1220–1232.